
# Electron Density Sharpening as a General Technique in Crystallographic Studies

**Chang Liu and Yong Xiong**

***Department of Molecular Biophysics and Biochemistry,*** *Yale University, New Haven, CT 06520-8114, USA*

***Correspondence to Yong Xiong:*** *yong.xiong@yale.edu*
http://dx.doi.org/10.1016/j.jmb.2013.11.014
***Edited by Y. Shi***

## Abstract

Sharpening is a powerful method to restore the details from blurred electron density in crystals with high overall temperature factors (*B*-factors). This valuable technique is currently not optimally used because of the uncertainty in the scope of its application and ambiguities in practice. We performed an analysis of ~2000 crystal data sets deposited in the Protein Data Bank and show that sharpening improves the electron density map in many cases across all resolution ranges, often with dramatic enhancement for mid- and low-resolution structures. It is effective when used with either experimental or model phases without introducing additional bias. Our tests also provide a practical guide for optimal sharpening. We further show that anisotropic diffraction correction improves electron density in many cases but should be used with caution. Our study demonstrates that a routine practice of electron density sharpening may have a broad impact on the outcomes of structural biology studies.



## Introduction

X-ray crystallography is the most powerful technique to determine the structures of macromolecules at the atomic level. The successful building of an atomic model relies on the quality and the effective resolution of the electron density map. Theoretically, atomic structure determination can be achieved at quite low resolution, as detailed side-chain information exists even at the resolution range 3.5–5 Å and only disappears at resolutions lower than 6 Å (Fig. 1a). In practice, only 1381 (1.6%) out of the over 84,000 structures currently deposited in the Protein Data Bank (PDB) [1] are solved at a resolution of 3.5–5 Å. The effective resolution of the electron density is often much lower than the resolution suggested by the diffraction limit of the measured data. Frequently, the diminishing of the apparent resolution is not caused by experimental or computational errors, as it occurs even when good-quality diffraction data are measured and excellent phases are obtained. This intrinsic loss of definition of the electron density can significantly hamper the structure determination and analysis that should have been achievable with the measured diffraction data.

The atomic displacement parameters (ADPs; temperature or *B*-factors) are used to describe the blurring of electron density due to the collective effect of many factors, such as thermal motion of the molecules, static defects in crystal packing, and non-ideal X-ray beam and detector responses [2–5]. The smearing effect is modeled as a convolution of the ideal electron density with a blurring Gaussian function, or point spread function, which also leads to the falloff of diffraction intensity as a function of resolution. Empirically, the average *B*-factor of well-diffracting crystals ranges from nearly 0 to 30 $Å^2$. It often becomes greater than 100 $Å^2$ for crystals diffracting to 3 Å or lower resolutions. The high *B*-factors cause a higher falloff rate of diffraction intensity at higher resolution and result in the loss of the detailed information that could have been observed at the nominal resolution if the molecule had lower ADPs (Fig. 1b). Because the overall ADPs can be different in different directions, anisotropic diffraction is commonly observed, resulting in a directional dependence of the diffraction intensity [3,6–8]. This may cause a smearing of the electron density along the direction of the weak data.

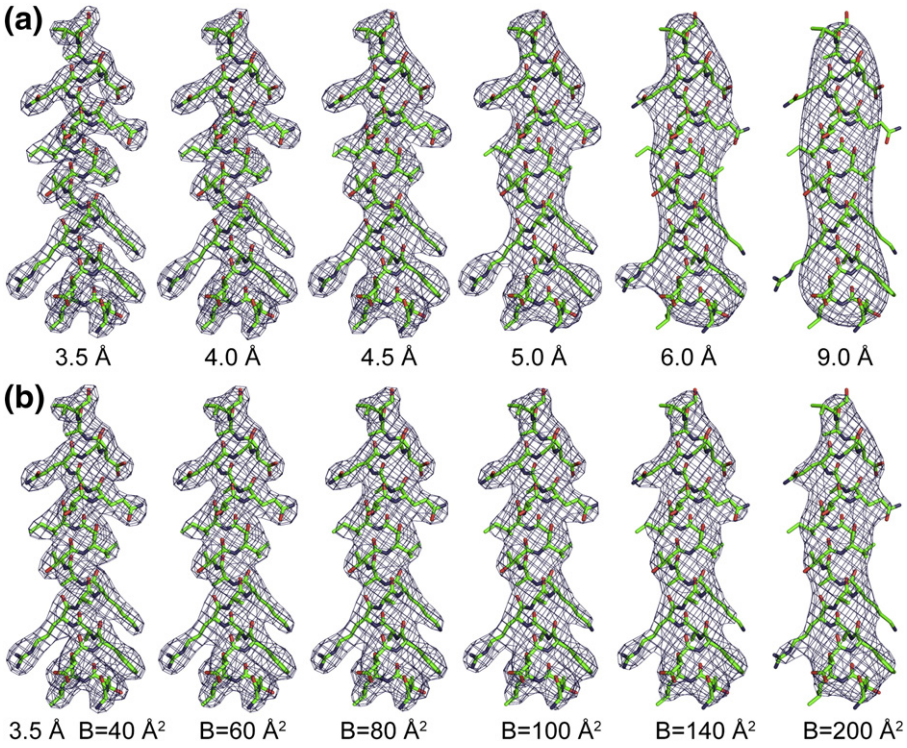


**Fig. 1.** Ideal electron density calculated from model amplitudes ($F_{calc}$) and model phases ($\phi_{calc}$) (a) at various resolutions with $B = 0$ Å$^2$ and (b) at 3.5 Å resolution with various $B$-factors. Electron density is shown in mesh, contoured at 1.0 sigma level, and the structural model is shown in stick.

The blurring effect can potentially be corrected by electron density sharpening. This method deconvolutes the blurring contribution from a global component of the ADPs through a modification to the observed diffraction data ($F_{obs}$). It was first introduced in the sharpening of Patterson functions to solve small molecule crystal structures by direct methods [9–11]. Because the blurring effect is described by a Gaussian function with a positive $B$-factor [Eq. (1)], the deconvolution can be conveniently achieved by applying a similar Gaussian function with a negative sharpening factor $b$ [Eq. (2)] [9,12–15]. The result of the deconvolution is the scaling up of the higher-resolution contribution of the data to recover the information lost by the blurring effect.

$$F_{obs} = F_{ideal} \cdot e^{-B\left(\frac{\sin\theta}{\lambda}\right)^2} \quad (\text{Temperature factor } B>0) \tag{1}$$

$$F_{sharpened} = F_{obs} \cdot e^{-b\left(\frac{\sin\theta}{\lambda}\right)^2} = F_{ideal} \cdot e^{-(B+b)\left(\frac{\sin\theta}{\lambda}\right)^2} \quad (\text{Sharpening factor } b<0) \tag{2}$$

A similar correction to anisotropic diffraction can be made by scaling the intensities in different directions to the same level [8,16,17]. The anisotropic correction is similar to sharpening, but it is applied through a tensor matrix with different values in different directions. In practice, anisotropic scaling is best achieved by fitting calculated amplitudes ($F_{calc}$) to $F_{obs}$ when an accurate model is available. This established method has been implemented in all major crystallographic refinement programs [18–21]. Alternatively, a prior correction can be achieved empirically by comparing $F_{obs}$ at different directions before a molecular model is available [8,22].

Despite its importance in solving small molecule structures by direct methods [9–11] and its proven success in many cases since its first documented application in macromolecular crystallography in 1996 [12], the optimal application of electron density sharpening has not been determined in macromolecular crystal structure studies. This is largely due to the uncertainty of its effectiveness and scope of application, the concern of introducing bias, and the ambiguity of the application procedure. The work reported herein addresses these questions by a thorough analysis of crystal structures and diffraction data deposited in the PDB. Our results demonstrate that electron density sharpening is a general, effective method that should be used routinely in the determination of crystal structures. The optimal sharpening procedure determined in this study may facilitate many crystallographic studies, especially challenging cases at mid to low resolutions.

## Results

### Sharpening is an effective method at all resolutions

We performed an analysis of 1982 crystal structures published in the journals *Cell*, *Nature*, *Science*, *Structure*, *Nature Structural and Molecular Biology*, and *Acta Crystallographica Section D* from 2008 to early 2011 that have diffraction data deposited in the PDB. Sharpening often resulted in a major enhancement of the electron density in this sampling pool (Fig. 2a–h and Table 1). We show that it is effective using either experimental (Fig. 2a and b) or model (Fig. 2c–h) phases in various space groups. It works on both protein and nucleic acid (Fig. 2c) crystals. As expected from the physical basis of the sharpening correction, the higher the overall temperature factor, Wilson *B*-factor [2], of the crystal is, the more dramatic the sharpening effect is. Most low-resolution crystals (e.g., >3 Å) have high *B*-factors (e.g., >60 Å$^2$) and often show large visual enhancement of the electron density after sharpening. In our survey, a vast majority of the low-resolution structures (334 out of 459 structures, or ~73% at resolution lower than 3 Å) have *B*-factors larger than 60 Å$^2$. In most of these cases, sharpening can make the side chains discernable for accurate model building.

The benefit of sharpening is not limited to low-resolution structures; it applies to crystals at all resolutions (Fig. 2f–h). Even in cases when the crystals diffracted to atomic resolutions of better than 1 Å, sharpening still results in significant improvement of the details of the electron density. Although molecular features such as side chains become commonly discernable at high resolutions, relatively high *B*-factors can still result in smeared electron density with the loss of expected details, such as holes in aromatic side chains (Fig. 2h). Sharpening in these mid- to high-resolution structural studies can recover the details and reveal defined side-chain rotamer conformations or even the geometry of the hydrogen atoms. This added detail leads to a much more precise model. This demonstrates the broad impact of sharpening in correcting an intrinsic blurring effect of electron density in crystallographic studies.

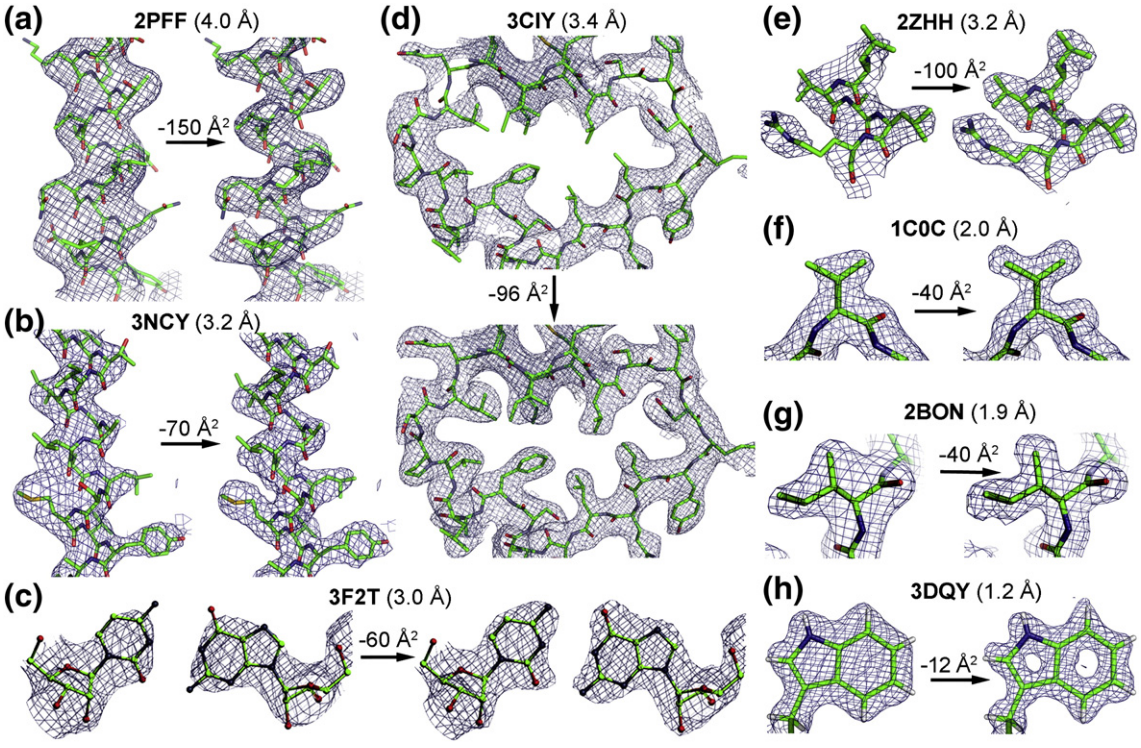


**Fig. 2.** Sharpening is a powerful technique to improve the electron density maps. Electron density is shown in mesh, contoured at 1.0 sigma level; structural models are shown in stick, and the PDB accession code is above each example. The arrows point from the original to the sharpened electron density. Sharpening works with experimental phases (a and b), model phases (c and h), protein or nucleic acid (c) crystals, and for a broad range of resolutions from 4 Å (a) to as high as 1.2 Å (h).

**Table 1.** Statistics of the crystal data used in the examples

| PDB ID | Resolution | Space group | Wilson *B* | Anisotropic *B* |
|---|---|---|---|---|
| 2PFF | 4.00 | $P4_32_12$ | 134 | 34 |
| 3CRW | 4.00 | $P2_12_12_1$ | 80 | 89 |
| 3CF2 | 3.50 | $P3$ | 70 | 76 |
| 1XXH | 3.45 | $P2_12_12_1$ | 91 | 69 |
| 3CIY | 3.41 | $C222_1$ | 107 | 15 |
| 3EHT | 3.40 | $P4_12_12$ | 132 | 1 |
| 3LVR | 3.38 | $P6_2$ | 91 | 65 |
| 3LVQ | 3.38 | $P6_2$ | 98 | 66 |
| 2XQ9 | 3.20 | $C2$ | 86 | 86 |
| 3NCY | 3.20 | $P1$ | 101 | 67 |
| 2ZHH | 3.20 | $P6_2$ | 137 | 97 |
| 3MHV | 3.10 | $P222_1$ | 86 | 59 |
| 2O93 | 3.05 | $P2_12_12_1$ | 67 | 50 |
| 3MH5 | 3.00 | $P6_322$ | 86 | 68 |
| 3HXR | 3.00 | $P2_12_12$ | 79 | 34 |
| 3F2T | 3.00 | $P312_1$ | 93 | 16 |
| 3BG1 | 3.00 | $C222_1$ | 89 | 73 |
| 3ECC | 2.70 | $P6_1$ | 47 | 54 |
| 2R02 | 2.60 | $C2$ | 64 | 54 |
| 2R88 | 2.60 | $C222_1$ | 47 | 23 |
| 3DVG | 2.60 | $C2$ | 58 | 26 |
| 3PEV | 2.5 | $P6_122$ | 47 | 55 |
| 3LFM | 2.50 | $H3$ | 61 | 21 |
| 3ETU | 2.4 | $P322_1$ | 50 | 43 |
| 2ZO0 | 2.19 | $P2_12_12_1$ | 62 | 67 |
| 1C0C | 2.00 | $P2_12_12_1$ | 43 | 10 |
| 2BON | 1.90 | $P2_1$ | 44 | 59 |
| 3KDJ | 1.88 | $P2_12_12_1$ | 36 | 32 |
| 3JY1 | 1.75 | $P2_1$ | 29 | 30 |
| 3DQY | 1.2 | $P2_1$ | 14 | 6 |

## Sharpening improves electron density maps with model-bias tolerance

Sharpening, as an amplitude correction technique, can be combined with any good estimate of phases to enhance electron density details. While its use with experimental phases has been accepted, uncertainty exists in the case of model phases because of potential model-bias issues. In theory, sharpening improves the amplitude component of the diffraction data and should not affect model bias that arises from the phase component. It is a modification on amplitude and retrieves the information stored in the measured diffraction data. When the phases are close to the correct values, the information stored in the amplitude reveals the true structure of the molecule despite moderate errors in the model. This phenomenon is in fact the basis of the difference Fourier method. In practice, however, the effectiveness of amplitude sharpening when using model phases and its effect on model bias has not been thoroughly studied.

Our sharpening tests show substantial unbiased improvement on electron density when using model phases (Fig. 2c–h), even when the model is incomplete and/or contains errors (Fig. 3). We used a model of maltose binding protein (MBP) (PDB accession 3HPI) to solve the crystal structure of an

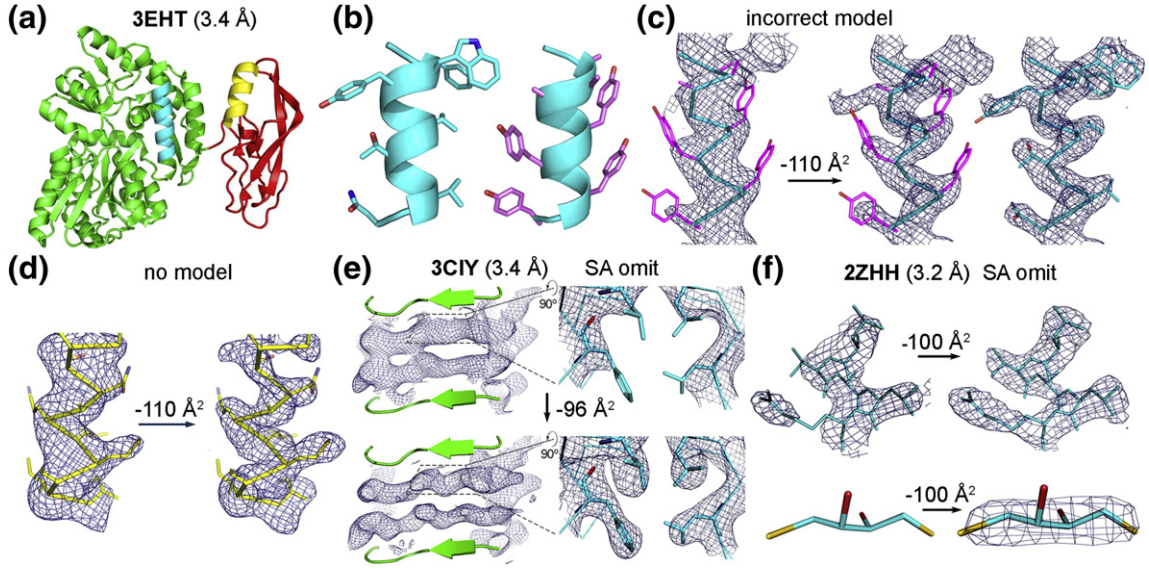


**Fig. 3.** Sharpening is effective using phases from incomplete models with errors. Electron density is shown in mesh, contoured at 1.0 sigma level; structural models are shown in stick, and the PDB accession code is above each example. The arrows point to sharpened electron density. Color code for stick model: green, model with phase information; cyan, incorrect or omitted model ; yellow, regions without model. (a) Final model of 3EHT. (b) The side chains of seven amino acids on an α-helix of 3EHT (left sub-panel) are inverted (right sub-panel, F/W/Y to A/A/A and V/V/T/N to Y/Y/Y/Y). (c) The density after sharpening reveals the correct 3EHT side-chain information even with the incorrect model phases. (d) Sharpening enhances the details of the electron density in a helical region (yellow) of 3EHT that does not have a model. (e and f) Sharpening enhances the electron density for the omitted part of the model. Two strands of 3CIY are omitted (left sub-panels) with a zoomed-in view of the details (right sub-panels) in (e). A helix and a ligand of 2ZHH are omitted in (f).

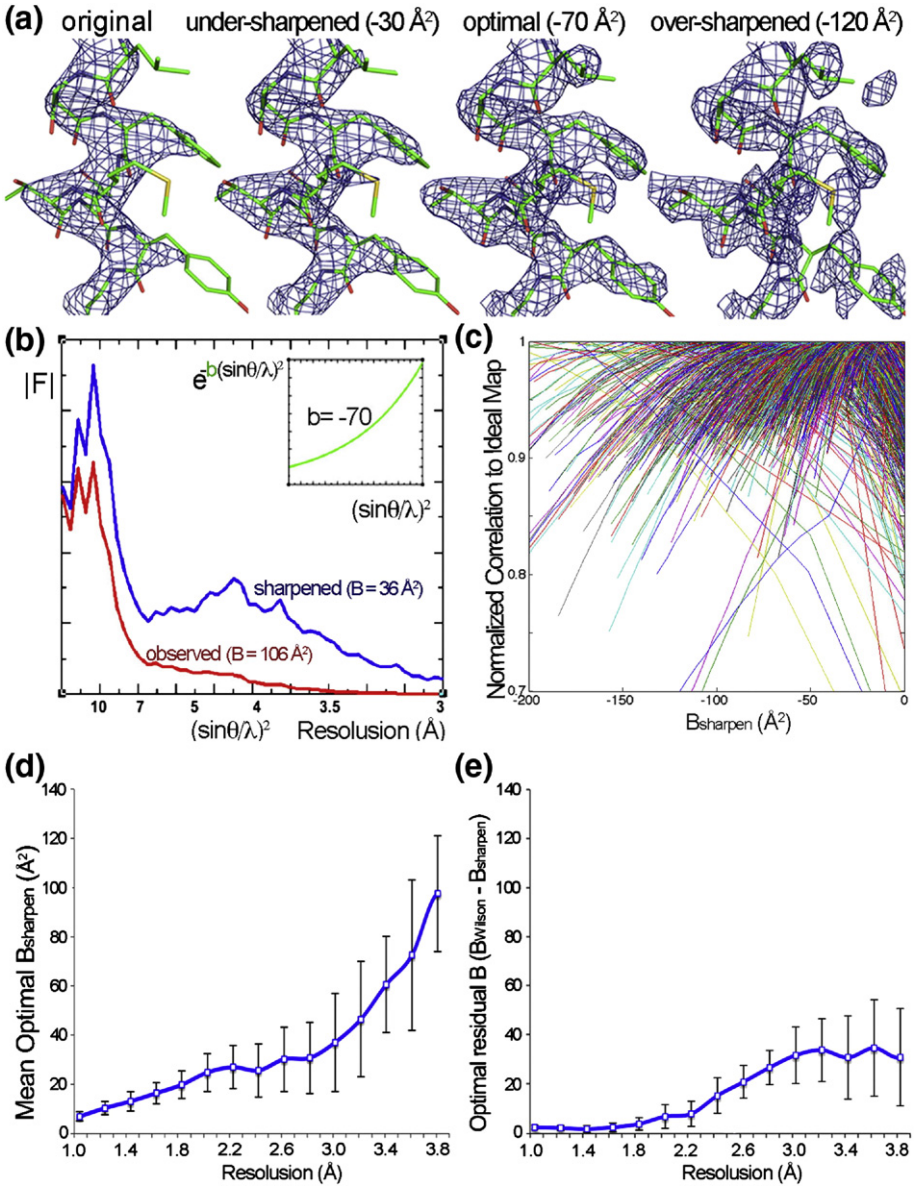


**Fig. 4.** Optimal sharpening factors. (a) Under-sharpening does not effectively improve the electron density and over-sharpening introduces noise. Electron density is shown in mesh, contoured at 1.0 sigma level; structural models are shown in stick. (b) Sharpening scales up the high-resolution part of the amplitude data. The original amplitude (red) is sharpened (blue) by a scaling function (green inset). (c) The correlation coefficient curves between the ideal model electron density and the Sigma-A weighted $2F_{obs} - F_{calc}$ maps with varying sharpening factors ($B_{Sharpen}$) for each of the 1982 test structures. The correlation coefficient is normalized to the maximum value in each case. The correlation curves show that an optimal $B_{harpen}$ (maximum correlation) exists for each structure. (d) Mean optimal sharpening factor plot and (e) mean residual *B*-factor ($B_{Wilson} - B_{sharpen}$) plot against the resolution limit of the diffraction data.

MBP-corticotropin-releasing factor (CRF) receptor fusion protein (PDB accession 3EHT) by molecular replacement (MR). The MBP-only model represents 75% of the fusion molecule (Fig. 3a). To further examine the potential model-bias problem, we introduced incorrect amino acids at seven positions on an α-helix in the MBP-only model where the relative sizes of the side chains are inverted (F/W/Y to A/A/A and V/V/T/N to Y/Y/Y/Y) (Fig. 3b). The MR solution using the modified MBP-only model was then refined to an *R*/*R*-free of 34.7%/37.4%. Notably, sharpening of the amplitude with a negative *B*-factor of −110 Å$^2$ resulted in an electron density map that unambiguously reveals the correct amino acid sizes even with the model phase calculated from the side-chain "inverted" model (Fig. 3c). Furthermore, sharpening substantially enhanced the details of the electron density in the CRF region that does not have a model

(Fig. 3d). This result clearly demonstrates that sharpening is a powerful technique even with significantly incomplete models and it does not increase model biases.

We also validated the use of sharpening with model phases by using simulated annealing (SA) omit maps [23,24], which is an effective technique for removing model bias. The results from 10 different test cases again confirm that sharpening with phases calculated from a partial model improves the electron density maps even for regions where the model is omitted (Fig. 3e and f). In some cases, it restores the electron density of bound ligands that are lost in the SA omit procedure (Fig. 3f). This underlines that sharpening functions to recover the amplitude information contributed from the less ordered components in the crystal, such as amino acid side chains and ligands. These SA omit map tests further confirm that the electron density map enhancement by sharpening is not due to model bias.

### Optimal sharpening factors—How much to sharpen

An optimal correction exists to account for the actual overall blurring effect in the crystal. Under-sharpening does not harness the full power of the method and over-sharpening may introduce artifacts (Fig. 4a). As the higher-resolution data are weaker and measured with a higher level of noise, their scaling up by sharpening (Fig. 4b) also escalates the noise. Because of this, over-sharpening can cause deterioration of the electron density [13]. A correction procedure has been implemented in REFMAC5 to regularize the noise amplified by sharpening [25]. In addition, over-sharpening can introduce Fourier termination errors, the so-called ripple or ringing effect, as the highest-resolution amplitudes are no longer close to zero. In practice, it is important to determine the appropriate sharpening factor that retrieves maximum details of the electron density without introducing significant noise or artifacts.

We investigated the optimal sharpening factors using a correlation-based method. The reference in the correlation calculation would ideally be from an electron density map that represents the true molecular image free of any blurring effect, which is obviously not available in practice. We chose the ideal reference map with the much simplified premise that the final refined model is error free and therefore the electron density map calculated with the model phases and amplitudes approximates the ideal molecular image. The *B*-factors of the ideal model are set to that of a "still" molecule (0 Å$^2$) so that the reference map yields the most details without any blurring effect. We downloaded the coordinates and diffraction data of 1982 crystal structures deposited in the PDB for the correlation-based sharpening tests. For each data set, we calculated the correlations between the ideal model electron density map and the Sigma-A weighted $2F_{obs} - F_{calc}$ maps sharpened with various *B*-factors. Results obtained from the much simplified approximation agree well with our thorough empirical inspection of electron density maps and are corroborated by the sharpening procedure implemented in the crystallographic package Phenix (discussed below). The results provide insight into the optimal sharpening factor that achieves the most improvement of the electron density map.

As expected, the correlation is a function of the degree of sharpening; it peaks at an optimal value and drops with either under-sharpening or over-sharpening (Fig. 4c). This assessment also verifies that sharpening indeed improves the electron density under nearly all circumstances (98%) (Table 2). The result showed a clear trend that the average optimal residual *B*-factor, $B_{Wilson} - B_{sharpen}$, is close to 0 Å$^2$ at high resolution (1.0–1.6 Å) and rises to 30–40 Å$^2$ at low resolution (3.0–3.8 Å) (Fig. 4d and e). Our results agree well with the automatic sharpening implemented in the autobuild protocol in Phenix, where the target *B*-factor (b_iso) is set to be 10 times of the value of the resolution [26]. This is more modest than the sharpening amount suggested by DeLaBarre and Brunger [13], where the sharpening *B*-factor is chosen to make the Wilson ratios $\ln(\langle F_o^2\rangle/\langle f_i^2\rangle)$ positive in all resolution shells. We also observed significant variations of optimal sharpening values at low resolution, with standard deviation of 20–30 Å$^2$ from the mean optimal residual *B*-factor (Fig. 4d and e). This is partly due to the intrinsic inaccuracy of estimating the Wilson *B*-factor at low resolution. The observed variations suggest that, in practice, it is advantageous to test a range of sharpening values around the average optimal value. These results offer a good practical guide for the initial sharpening values to be applied and ranges to be tested for a new data set to gain the best improvement of the electron density map. Furthermore, different sharpening factors may be applied to improve different parts of the molecules in the crystal, as they may not have the same extent of displacement or motion. The graphic program Coot has implemented a sharpening tool that conveniently adjusts the amount of sharpening on the displayed electron density.

### Sharpening in practice—When to sharpen

Although sharpening is an amplitude correction technique, its power increases when the accuracy of the phases improves. This is a direct consequence of Fourier transform; a good final synthesis with improved amplitude still requires good phases. This has important practical consequences. Often sharpening does not appear to be very effective at the beginning of structure determination, when phase

**Table 2.** Changes in map correlation after sharpening or anisotropic correction

| | Sharpening | | Intensity-based anisotropic correction | | | |
|---|---|---|---|---|---|---|
| | | | All | | Highly anisotropic ($\Delta B > 40$ Å$^2$) | |
| Correlation[a] coefficient | Percentage (%) | Number of structures | Percentage (%) | Number of structures | Percentage (%) | Number of structures |
| Increase | 98.0 | 1943 | 63.1 | 1250 | 90.0 | 180 |
| Decrease | 0.6 | 11 | 26.0 | 516 | 10 | 20 |

[a] Correlation coefficient (CC) is calculated between an ideal model map and the Sigma-A weighted $2F_{obs} - F_{calc}$ map. The CC calculated with the original electron density is compared with the CC calculated with the map sharpened with the optimal *B*-factor (Fig. 4c) with or without correction for anisotropy.

errors are large. However, its ability to improve electron density becomes more significant and critical when phases become more accurate at later stages. This also emphasizes the practical aspect that although sharpening does not increase model bias, as we have shown above, its effectiveness can be affected when there is substantial model bias, that is, significant phase errors.

We first demonstrated the dependency of sharpening on the quality of experimental phases using a real case study of the crystal structure of the *Salmonella* arginine transporter AdiC at 3.2 Å resolution (Fig. 5a and b) [27]. The initial phases were obtained using the multi-wavelength anomalous dispersion method with a figure of merit (FOM) of 0.35, corresponding to an average phase error of

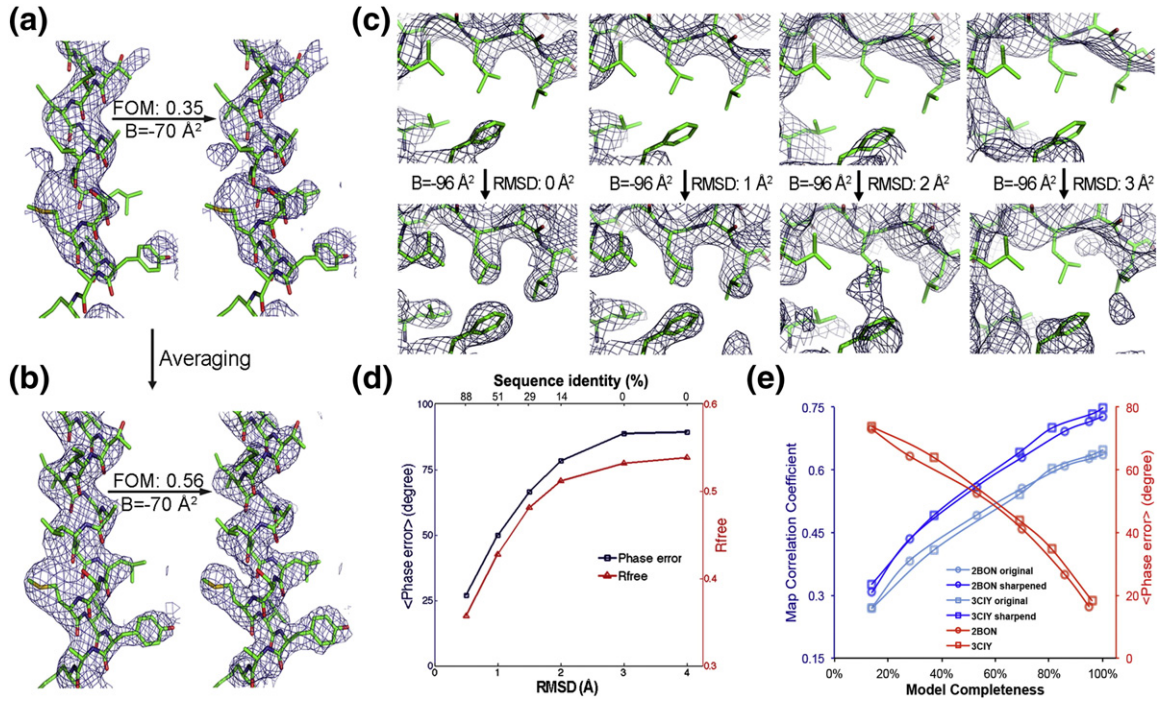


**Fig. 5.** The effect of sharpening with phase errors. (a and b) Sharpening has little effect on electron density when the experimental phase quality is poor (FOM = 0.35) (a) but significantly enhances electron density when the phases are improved (FOM = 0.56) (b). Electron density is shown in mesh, contoured at 1.0 sigma level, and the structural model is shown in stick. (c) The effect of sharpening with increasing phase errors generated by introducing random coordinate errors (RMSD = 0–4 Å). Sharpening is more effective when the phase errors are small. (d) The phase errors (black) relative to the original structure and *R*-free factors (red) generated by the randomized coordinates in (c). (e) The effect of sharpening with increasing phase errors generated by decreasing model completeness. The correlation coefficients between the electron density map calculated from an ideal model and those from truncated models are plotted, with unsharpened data in light blue and sharpened data in blue. The mean phase errors for the truncations are plotted in red.

~70°. Sharpening did not improve the electron density at this stage (Fig. 5a). In contrast, sharpening significantly enhanced the details of the electron density map after the phases had been improved by multi-crystal averaging (FOM = 0.56, average phase error ~ 55°) (Fig. 5b). The sharpened electron density map is critical for the success of model building, which in turn further improved the sharpened map when the experimental phases were combined with those calculated from the well-refined model [27].

We also confirmed a correlation of the power of sharpening to the phase quality (Fig. 5c and d) in a test case where we simulated model phase errors by randomizing ("shaking") the coordinates of the final refined model with root-mean-square deviations (RMSD) from 0 to 4 Å. The results show a clear inverse correlation between the electron density enhancing ability of sharpening and the amount of phase errors (Fig. 5c and d). Interestingly, sharpening appears to be able to tolerate relatively large phase errors. It is still effective with a coordinate error of RMSD = 1.5 Å, corresponding to a model with sequence identity of ~30% [28] and phase error of about 60° (Fig. 5c and d). The positive sharpening effect is lost when the RMSD is bigger than 2 Å (phase error of ~75° and sequence identity of ~15%).

We further tested the effectiveness of sharpening with phase errors generated by incomplete models. We generated models with various amounts of truncations (0–90%), refined the truncation models by SA, and calculated the correlations between the electron density map computed from the ideal model and those from the refined truncation models with or without sharpening (Fig. 5e). As expected, the result shows that the power of sharpening, indicated by an improvement in map correlation, decreases with increasingly incomplete model. When the models are 40–50% complete, corresponding to a mean phase error of ~60°, the electron density can still be enhanced by sharpening. This result is consistent with the test mentioned above using randomized coordinates (Fig. 5d). Taken together, the test results using experimental phases and phases from randomized or incomplete models suggest that, in practice, sharpening may not be helpful at the beginning of structure determination when phase errors are large. An increasing amount of sharpening can be applied during the course of the structure refinement and phase improvement to achieve electron density enhancement.

## Target of sharpening—What to modify

As sharpening is essentially an image processing technique applied to electron density maps in the Fourier space, the most straightforward practice is to apply the modification to the Fourier coefficients, that is, the Sigma-A weighted map coefficients. The technique improves electron density maps and the crystallographic processes directly related, such as map interpretation and model building. Density modification processes may also be improved by sharpening of map coefficients because of the increased definition in the molecular image after sharpening. This is performed by default in many density modification procedures (e.g., DM [29]).

Sharpening of $F_{obs}$ is not expected to affect the phasing and refinement calculations, as the refinement targets are functions of $F_{obs}/\sigma_{Fobs}$, which remain unchanged when both $F_{obs}$ and $\sigma_{Fobs}$ are sharpened by the same multiplication factor. In fact, the maximum likelihood target in these calculations can be expressed as a function of the normalized structure factor E [30–32], which removes any resolution-dependent decay of the amplitude [33,34], including the *B*-factor effect and the resolution-dependent falloff of scattering factors due to the physical sizes of the atoms. This implementation essentially includes a variation of the sharpening correction. In fact, sharpened $F_{obs}$ will lead to an apparent increase in the refinement *R*-factors. As the relatively more noisy, higher-resolution data are scaled up by sharpening (Fig. 4b), their contributions to the overall *R*-factor calculation become larger, even though the model quality does not change. We compared the results of sharpening on $F_{obs}$ before refinement and on map coefficient after refinement using our sample pool. As expected, the improvement of the electron density maps does not differ between the two ways of sharpening, while sharpening on $F_{obs}$ increases the apparent *R*-factors.

## Sharpening improves model building

A direct consequence of electron density improvement by sharpening is less uncertainty in map interpretation and reduced difficulty in high-quality model building, especially at mid to low resolutions. The enhancement of the electron density details is evident by visualization (Fig. 2). We further used the automated model-building programs Buccaneer [35] and Phenix [36] as an objective assessment of the sharpening improvement in model building. We compared the models built with and without sharpening, using the automated building-refinement protocols implemented in the programs, for 19 structures at various resolutions ranging from 1.7 Å to 3.5 Å. The results show that sharpening leads to improved models automatically built in the majority of the test cases, often with significantly lower *R*-free values (Fig. 6). In some cases, it is critical for successful model building. For example, *R*-free values of 27% *versus* 50% were obtained for models built with or without sharpening (Fig. 6a). The effect of sharpening on model building with high-resolution data was less significant than that for low-resolution cases, as *R*-free values were often already low for the models built without sharpening, although further improvement was observed after

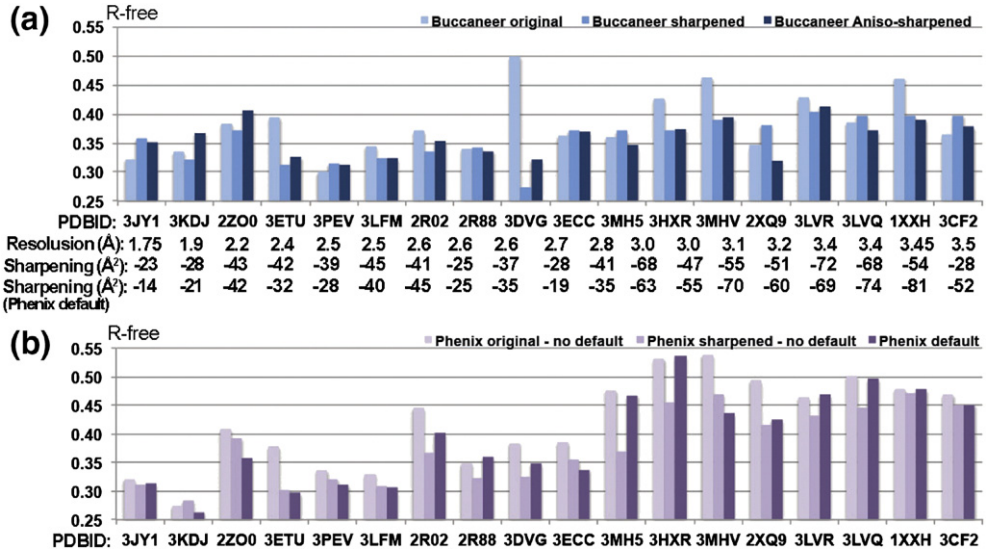


**Fig. 6.** Automated model building with original, sharpened, or sharpened and anisotropy-corrected data. (a) Results after automated model building using Buccaneer. The results from the original, sharpened, and sharpened plus anisotropy-corrected data are shown in light blue, blue, and dark blue, respectively. The corresponding PDB ID, resolution, and sharpening amount in each case are labeled below the graph. (b) Results after automated model building using Phenix autobuild. The results from the original, non-default sharpened, and default sharpened plus anisotropy-corrected data are shown in light purple, purple, and dark purple, respectively. The non-default sharpening values are the same as those shown in (a), and the default sharpening values are shown above the graph.

sharpening. Sharpening frequently increases the number of side chains correctly built and the lengths of continuously built chains, ultimately leading to better-quality models.

We further analyzed model building using the autobuild protocol implemented in Phenix, as it includes data sharpening and anisotropic correction by default. The automated routine performed well in general, especially at resolutions higher than 3 Å (Fig. 6b). Importantly, an improvement beyond the default procedure could often be observed using manually sharpened data with different sharpening values (Fig. 6b). Although the non-default calculations do not include anisotropic correction as in the default cases, the improvement is not due the lack of this correction, as anisotropic correction on the contrary often leads to the improvement of electron density map and the model built. This is shown in the test cases with Buccaneer (Fig. 6a) and discussed below. The improvement in the non-default tests is therefore due to the different sharpening values. This is consistent with our results discussed above that the optimal sharpening factors often deviate from the predicted average values and a range of values should be tested in practice.

## Anisotropic *B*-factor correction can improve electron density and the effect of sharpening

Diffraction from a crystal is in general anisotropic, as the strength of lattice contacts typically varies in different directions, except for those in the cubic space group. The anisotropic effect manifests in different rates of intensity falloff along different directions in the diffraction, which leads to the smearing of the electron density along the directions with higher falloff rate (Fig. 7a). The anisotropic effect is modeled with an ellipsoidal *B*-factor tensor and can be treated in a number of ways [3,6,7]. It has been established that the overall anisotropic scaling of $F_{calc}$ to $F_{obs}$ has a significant effect on macromolecular refinement [17] and the procedure has been incorporated in all major refinement programs [18–21]. Alternatively, an intensity-based anisotropic correction without model information can be applied, by a procedure similar to sharpening, to have the same *B*-factors values in all directions and isotropic resolution-dependent intensity falloff (Fig. 7a). The correction can potentially remove the smearing and restore the details in electron density (Fig. 7a and b). This has been shown to improve refinement and the electron density map, and the correction has been implemented in a Web server[†] [8].

We investigated the intensity-based anisotropic correction, and the result shows that the correction improves the electron density in many highly anisotropic structures and often facilitates sharpening (Table 2) (Fig. 7b). We used Phaser [22] to perform anisotropic correction of the diffraction from the 200 crystals in our sampling pool where the anisotropic $\Delta B$-factors are larger than 40 Å$^2$. Improvement of the electron density map was observed in many cases. Furthermore, for the highly anisotropic diffractions, sharpening alone often does

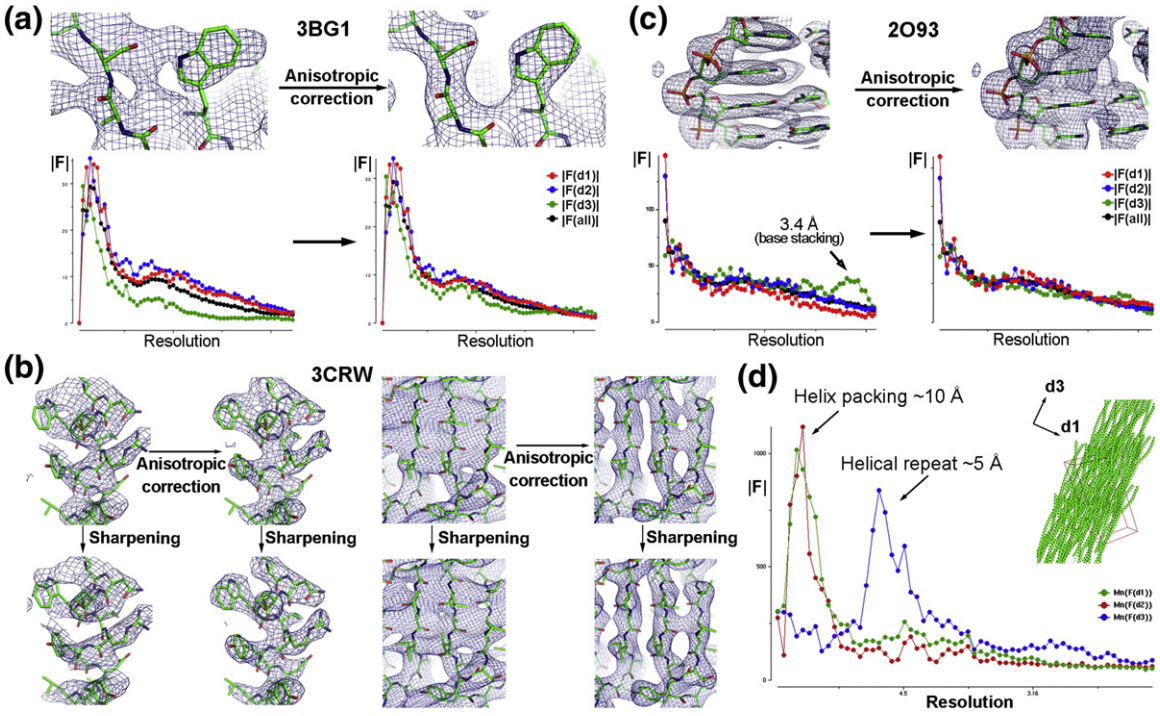


**Fig. 7.** The effects of anisotropic correction and sharpening. (a) Anisotropic correction enhances electron density (top) and changes the diffraction intensity in different directions to the same falloff rate (bottom). The smearing along the direction of weak diffraction (d3, green curve on the bottom) is removed after the correction. Electron density is shown in mesh, contoured at 1.0 sigma level, and the structural models are shown in stick. (b) Sharpening only improves the electron density after the anisotropic correction. Two example regions of the electron density are shown on the left and right. (c) Inappropriate application of anisotropic correction can lead to the deterioration of the electron density. The correction removes the intrinsic signal from DNA base stacking, which gives rise to a false apparent anisotropy at ~3.4 Å. (d) Example of repeating structural motif that generates non-uniform diffractions. The crystal packing of the coiled-coil structure of tetherin/BST2 [37] is shown on right. The α-helices line up in the same direction. The interference of the non-crystallographic repeating units generates modulations of the diffraction intensity in the repeat direction at resolutions consistent with the dimensions of the repeating units.

not change the smeared appearance of the electron density map, while sharpening on the anisotropy-corrected diffraction significantly enhances the details in the map (Fig. 7b). This is also demonstrated in our automated model-building test in Buccaneer and Phenix, where anisotropic correction plus sharpening led to much improved models in some cases (Fig. 6a).

### Caveats on anisotropic correction

Our test also shows that intensity-based anisotropic correction reduced the quality of the electron density map in a significant number of the cases, indicating that caution is needed when applying the correction. It is possible that an apparent anisotropic intensity distribution is the result of an intrinsic property of an isotropically diffracting crystal. For example, when repeating structural motifs line up in a crystal, such as DNA duplexes or α-helices [37], constructive interferences enhance the diffraction intensity along the repeat direction at a resolution equal to the repeat distance (Fig. 7c and d). The interference effect gives rise to an anisotropic appearance of the diffraction at particular resolutions, such as the intensity increase at ~3.4 Å resolution due to DNA base stacking (Fig. 7c). This could be mistaken as anisotropic diffraction of the crystal. When the intensity-based modification is applied to remove this intrinsic diffraction feature, it may lead to the deterioration of the electron density (Fig. 7c). This caveat is also corroborated in our automated model-building test in Buccaneer and Phenix, where anisotropic correction plus sharpening lead to deteriorated models in some cases (Fig. 6a).

## Discussion

The quality and details of the electron density map are critical for successful building of an accurate molecular model, the fundamental goal of a crystallographic experiment. At the resolution defined by the diffraction limit of the data, even with the best-measured amplitudes and good phases, the spatial definition of the electron density map depends on a blurring effect manifested in the resolution-dependent falloff of the

amplitudes. The effect is essentially the same as that described by the ADPs, with the practical difference being that it is a collective effect from all parts or major regions of the molecule. Electron density sharpening corrects the smearing effect by applying a negative Gaussian to deconvolute the blurring function from the electron density. This interpretation of the physical basis of sharpening explains why the correction is beneficial. For a simplified example, if the blurring caused by the overall vibration of a molecule is removed, a still image that is stored in the measured data with better definition will be recovered.

Sharpening has long been shown to be effective, with the first documented application in macromolecular crystallography in 1997 [12] and the implementation in the CCP4 crystallographic program CAD [38] well over a decade ago. The technique has recently been implemented in many major software packages, such as CNS [19,20], Phenix [36], Coot [39], and REFMAC5 [31]. We surveyed the 4531 structures published between January 2008 and September 2013. Only 116 (2.6%) structures explicitly reported the use of the sharpening method. Many of these structures may have benefited from the automated sharpening procedures in the programs without being reported. However, this may also mean that sharpening has not become a common practice in the structural biology community beyond the program defaults, especially at low resolutions where sharpening is most powerful but the automated modeling is not yet effective. The lack of use is presumably because of the uncertainty of its usefulness and how to apply the correction without introducing artifacts.

Herein we show that sharpening is a general and powerful method for restoring the details of electron density maps that are lost due to the blurring effect. Sharpening improved electron density in most of the test cases. Our tests show that optimal sharpening depends on the resolution limit of the crystal and on average should leave a small residual *B*-factor, but with case-by-case variations. The phasing information can be from experimental phasing, density modification, or MR with a reasonable model. In practice, care should be taken regarding model bias when using MR phases. However, it should be pointed out that model bias is an intrinsic, sharpening-independent crystallographic problem. Sharpening improves the amplitude component of the electron density equation, which is independent to the model bias arising from the phase component (Fig. 3). In the cases when the unmeasured "missing" amplitudes are filled with the $F_{calc}$ calculated with the model, as implemented in many modern refinement programs, model bias is embedded to some degree in the amplitude components, too. Sharpening in these cases will simply allow the details to be seen clearer; it does not reduce or increase model bias. In fact, sharpening often has little effect when the phase quality is poor and becomes more effective when phases are improved (Fig. 4). On the other hand, even high-quality phases may not yield good electron density without sharpening. It is therefore important to use the technique to obtain the best electron density map allowed by the data, which will in turn lead to improved models and phases.

Anisotropic correction of the diffraction intensity can be considered as a special form of sharpening; that is, the sharpening factor is direction dependent. It improves electron density in most of the highly anisotropic cases in our test. Caution should be exercised when there are significant repeating structural features in the crystal, such as DNA duplexes or coiled-coil helices, whose interference effect may lead to the redistribution of the otherwise isotropic diffraction intensity. Such intrinsic diffraction may result in a false anisotropic appearance that should not be corrected. In practice, fortunately, most macromolecules contain more or less randomly distributed structural elements and the anisotropic correction on the diffraction data should be tested.

Although effective in most cases, the existing sharpening algorithm simplistically treats the entire asymmetric unit of the crystal as one rigid group. Macromolecules often have domains with different mobility (Fig. 8). The flexibility of these domains results in their blurred or diminished local electron density, which cannot be corrected effectively using the current overall sharpening methods. Domain-wise sharpening methods are needed to improve this technique. The TLS (*t*ranslation/*l*ibration/*s*crew) refinement has been shown to be highly successful in modeling the domain-wise motions [3,43,44]. However, it models but does not correct the smearing effect. As a consequence, although it reduces the refinement *R*-factors significantly, small improvement has been observed in the resulting electron density map. Ideally, the TLS parameters can be used to achieve domain-wise deconvolution of the displacements, which is a topic of future research.

A common and routine practice of sharpening will have a significant impact on the outcomes of structural biology studies. Our study provides a practical guide for optimal sharpening. In practice, the largest impact of sharpening is on the mid- to low-resolution structures, where enhanced detail of electron density is crucial for successful structure determination and atomic model building. The enhancement reduces the uncertainty of main-chain connectivity and side-chain assignment, which often require tremendous effort and guesswork at low resolution. Limited resolution is likely a growing problem as structural biology moves onto the next stage, namely, targeting large macromolecular complexes. While crystals of these complexes may be obtained, they typically only diffract to low resolutions. A broader application of sharpening, which facilitates harnessing the full potential of the

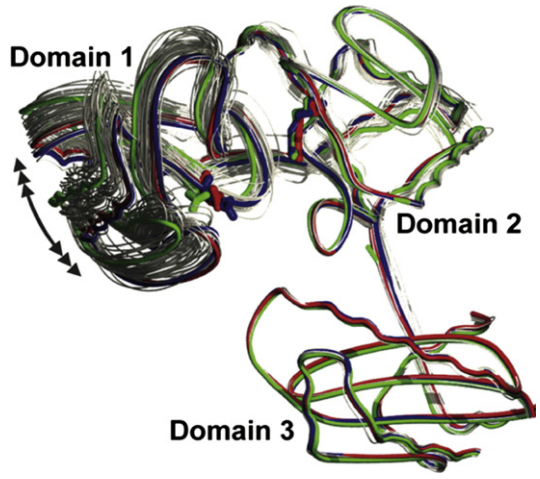


**Fig. 8.** Overlay of 39 independent copies of CCA-adding enzyme molecules in various crystals [40–42] shows that it has one flexible and two stable domains.

diffraction data, will help us to expand the capacities of structural studies.

## Materials and Methods

### Survey sampling pool

A total of 4531 structures were published from January 2008 to September 2013 in six journals, including *Cell*, *Nature*, *Science*, *Structure*, *Nature Structural and Molecular Biology*, and *Acta Crystallographica Section D*. The publications were scanned for the keywords such as "sharpen", "negative", "*B*-factor", "temperature factor", or "scaling", and the methods sections were inspected thoroughly to determine whether sharpening was applied in the studies.

### *B*-factor estimation and map sharpening

Coordinates and diffraction data of 1982 crystal structures were downloaded from the PDB for sharpening tests. Wilson *B*-factors were estimated using Phaser [22]. Sigma-A weighted $2F_{obs} - F_{calc}$ map coefficients (FWT) and phases are calculated from the deposited data and coordinates using REFMAC5 [21,31]. Sharpening modifications to $F_{obs}$ or FWT were carried out using the CCP4 program CAD [38] in which the negative value of the sharpening *B*-factor was input under the keyword "SCALE". Sharpening factors were varied from 0 to 1.5 times of Wilson *B* to determine the optimal value and test the effects of under-sharpening and over-sharpening. Electron density maps were displayed using Coot [39] for visual inspection of the sharpening effect.

### Map correlation

The sharpening effect was quantified by using the correlation coefficient between the FWT map and an ideal model map. The ideal reference model map coefficients ($F_{calc}$) and phases ($\phi_{calc}$) were calculated from the final refined model with *B*-factors set to 0, by using the CCP4 program SFALL [45]. The electron density maps were generated using the CCP4 program FFT [46]. Correlation of the maps was calculated using MAPMAN [47].

### Model-bias test

The MBP (PDB accession 3HPI) model was manually modified in Coot to introduce incorrect amino acids where the relative sizes of the side chains are inverted (F/W/Y to A/A/A and V/V/T/N to Y/Y/Y/Y) (Fig. 3b). The modified MBP model was used to solve the crystal structure of an MBP-CRF receptor fusion protein (PDB accession 3EHT) by MR using Phaser. The MR solution obtained with the modified MBP model was then refined to an *R*/*R*-free of 34.7%/37.4% using REFMAC5 without any manual rebuilding. The resulting maps were compared with or without sharpening.

To generate SA omit maps, we manually deleted a region of the test structures, such as a helix, several strands, or ligands, in Coot. SA was performed on the modified models using the Phenix software package by default settings (start_temperature = 5000, final_temperature = 300, cool_rate = 100, and number_of_steps = 50). The resulting maps were compared with or without sharpening.

### Phase error analysis

Experimental phasing by multi-wavelength anomalous dispersion and density modification by multi-crystal averaging for the AdiC structure were described previously [27]. The model phase errors were simulated by randomizing the coordinates of the final refined model with RMSD values from 0 to 4 Å, calculated using the "sites.shake = n" (n is the RMSD to be generated) command in the Phenix software package [18]. The mean phase error generated by each "shaking" was calculated using CCP4 program cphasematch [48]. The sequence identity was converted from the RMSD by using the published method [28]: Identity% = [ln(RMSD/0.4)]/1.87. The *R*-free factor of each model with errors was calculated using REFMAC5 without any refinement.

To test the effect of model incompleteness, we generated a series of model truncations in Coot by manually deleting 5–90% of the model structure, rendering the completeness from 95% to 10%. The truncated models are refined with simulated anneal in Phenix. The resulting maps, with or without sharpening, were used to calculate map correlation with the ideal reference model map.

### Automated model building

Auto-building was performed using the CCP4 program Buccaneer [35,49] and Phenix autobuild [36]. Both methods were running with the default fast mode or quick mode settings. The starting phases for auto-building were calculated from the final refined model. The original, sharpened, and anisotropic corrected plus sharpened $F_{obs}$ were tested for comparisons. The sequence of the protein was given for the building of the side chains. The resulting models were refined by REFMAC5 as a built-in routine in

the Buccaneer process without manual intervention. Phenix was also used to carry out auto-building with default settings. The amount of sharpening in Phenix default was retrieved from the log files. For the non-default Phenix autobuild process, the default anisotropic correction and sharpening option was turned off to compare the autobuild results using the original or manually sharpened $F_{obs}$. To meaningfully compare the results, we calculated all the *R*-free factors from the auto-refined models with unsharpened data.

### Anisotropic diffraction correction

The anisotropic Δ*B*-factors were estimated using Phaser. The intensity-based anisotropic correction was performed using Phaser without model information. The changes in the correlation to the ideal model map before and after the correction were calculated as described above. The intensity falloff plots were generated using CCP4 program ctruncate [50].

## Acknowledgments

We thank Jimin Wang and Garib Murshudov for insightful discussions and Jennifer Fribourgh, Henry Nguyen, and Erin Weber for comments on the manuscript.

*Received 2 August 2013;*
*Received in revised form 12 November 2013;*
*Accepted 14 November 2013*
Available online 21 November 2013

***Keywords:***
B-factor sharpening;
anisotropic correction;
automated model building;
phase error tolerance;
model-bias tolerance

† http://services.mbi.ucla.edu/anisoscale

***Abbreviations used:***
ADP, atomic displacement parameter; MBP, maltose binding protein; CRF, corticotropin-releasing factor; MR, molecular replacement; SA, simulated annealing; FOM, figure of merit.

## References

[1] Berman HM, Westbrook J, Feng Z, Gilliland G, Bhat TN, Weissig H, et al. The Protein Data Bank. Nucleic Acids Res 2000;28:235–42.
[2] Wilson A. Determination of absolute from relative X-ray intensity data. Nature 1942;150:151–2.
[3] Cruickshank D. The analysis of the anisotropic thermal motion of molecules in crystals. Acta Crystallogr 1956;9:754–6.
[4] Dunitz JD, Maverick EF, Trueblood KN. Atomic motions in molecular crystals from diffraction measurements. Angew Chem Int Ed Engl 1988;27:880–95.
[5] Trueblood KN, Burgi HB, Burzlaff H, Dunitz JD, Gramaccioli CM, Schulz HH, et al. Atomic displacement parameter nomenclature. Report of a subcommittee on atomic displacement parameter nomenclature. Acta Crystallogr Sect A Found Crystallogr 1996;52:770–81.
[6] Sheriff S, Hendrickson WA. Description of overall anisotropy in diffraction from macromolecular crystals. Acta Crystallogr Sect A Found Crystallogr 1987;43:118–21.
[7] Grosse-Kunstleve RW, Adams PD. On the handling of atomic anisotropic displacement parameters. J Appl Crystallogr 2002;35:477–80.
[8] Strong M, Sawaya MR, Wang S, Phillips M, Cascio D, Eisenberg D. Toward the structural genomics of complexes: crystal structure of a PE/PPE protein complex from *Mycobacterium tuberculosis*. Proc Natl Acad Sci USA 2006;103:8060–5.
[9] Patterson AL. A direct method for the determination of the components of interatomic distances in crystals. Z Kristallogr 1935;90:517–42.
[10] Wunderlich J. A new expression for sharpening Patterson functions. Acta Crystallogr 1965;19:200–2.
[11] Rossmann MG, Arnold E. Patterson and molecular-replacement techniques. Int Tables Crystallogr, B; 2006 235–63.
[12] Stehle T, Gamblin SJ, Yan Y, Harrison SC. The structure of simian virus 40 refined at 3.1 Å resolution. Structure 1996;4:165–82.
[13] DeLaBarre B, Brunger AT. Considerations for the refinement of low-resolution crystal structures. Acta Crystallogr Sect D Biol Crystallogr 2006;62:923–32.
[14] Brunger AT, DeLaBarre B, Davies JM, Weis WI. X-ray structure determination at low resolution. Acta Crystallogr Sect D Biol Crystallogr 2009;65:128–33.
[15] Patterson AL. A Fourier series method for the determination of the components of interatomic distances in crystals. Phys Rev 1934;46:372–6.
[16] Hughes EW. The crystal structure of melamine. J Am Chem Soc 1941;63:1737–52.
[17] Murshudov GN, Davies GJ, Isupov M, Krzywda S, Dodson EJ. The effect of overall anisotropic scaling in macromolecular refinement. CCP4 Newsletter on Protein Crystallography, 35; 1998 37–42.
[18] Afonine PV, Grosse-Kunstleve RW, Echols N, Headd JJ, Moriarty NW, Mustyakimov M, et al. Towards automated crystallographic structure refinement with phenix.refine. Acta Crystallogr Sect D Biol Crystallogr 2012;68:352–67.
[19] Brunger AT, Adams PD, Clore GM, DeLano WL, Gros P, Grosse-Kunstleve RW, et al. Crystallography & NMR system: a new software suite for macromolecular structure determination. Acta Crystallogr Sect D Biol Crystallogr 1998;54:905–21.
[20] Brunger AT. Version 1.2 of the crystallography and NMR system. Nat Protoc 2007;2:2728–33.
[21] Murshudov GN, Skubak P, Lebedev AA, Pannu NS, Steiner RA, Nicholls RA, et al. REFMAC5 for the refinement of macromolecular crystal structures. Acta Crystallogr Sect D Biol Crystallogr 2011;67:355–67.
[22] McCoy AJ, Grosse-Kunstleve RW, Adams PD, Winn MD, Storoni LC, Read RJ. Phaser crystallographic software. J Appl Crystallogr 2007;40:658–74.
[23] Brünger AT, Kuriyan J, Karplus M. Crystallographic R factor refinement by molecular dynamics. Science 1987;235:458–60.

[24] Brunger AT, Adams PD. Molecular dynamics applied to X-ray structure refinement. Acc Chem Res 2002;35:404–12.
[25] Nicholls RA, Long F, Murshudov GN. Low-resolution refinement tools in REFMAC5. Acta Crystallogr Sect D Biol Crystallogr 2012;68:404–17.
[26] Terwilliger TC, Grosse-Kunstleve RW, Afonine PV, Moriarty NW, Zwart PH, Hung L-W, et al. Iterative model building, structure refinement and density modification with the PHENIX AutoBuild wizard. Acta Crystallogr Sect D Biol Crystallogr 2008;64:61–9.
[27] Fang Y, Jayaram H, Shane T, Kolmakova-Partensky L, Wu F, Williams C, et al. Structure of a prokaryotic virtual proton pump at 3.2 Å resolution. Nature 2009;460:1040–3.
[28] Chothia C, Lesk AM. The relation between the divergence of sequence and structure in proteins. EMBO J 1986;5:823–6.
[29] Cowtan K. "dm": an automated procedure for phase improvement by density modification. Joint CCP4 and ESF-EACBM Newsletter on Protein Crystallography, 31; 1994. p. 34–8.
[30] Pannu NS, Read RJ. Improved structure refinement through maximum likelihood. Acta Crystallogr Sect A Found Crystallogr 1996;52:659–68.
[31] Murshudov GN, Vagin AA, Dodson EJ. Refinement of macromolecular structures by the maximum-likelihood method. Acta Crystallogr Sect D Biol Crystallogr 1997;53:240–55.
[32] McCoy A. Liking likelihood. Acta Crystallogr Sect D Biol Crystallogr 2004;60:2169–83.
[33] Karle J, Hauptman H. Application of statistical methods to the naphthalene structure. Acta Crystallogr 1953;6:473–6.
[34] Subramanian V, Hall SR. Normalized structure factors. I. Choice of scaling function. Acta Crystallogr Sect A Cryst Phys Diffr Theor Gen Crystallogr 1982;38:577–90.
[35] Cowtan K. The Buccaneer software for automated model building. 1. Tracing protein chains. Acta Crystallogr Sect D Biol Crystallogr 2006;62:1002–11.
[36] Adams PD, Afonine PV, Bunkoczi G, Chen VB, Davis IW, Echols N, et al. PHENIX: a comprehensive Python-based system for macromolecular structure solution. Acta Crystallogr Sect D Biol Crystallogr 2010;66:213–21.
[37] Yang H, Wang J, Jia X, McNatt MW, Zang T, Pan B, et al. Structural insight into the mechanisms of enveloped virus tethering by tetherin. Proc Natl Acad Sci 2010; 107:18428–32.
[38] Collaborative Computational Project, Number 4. The CCP4 suite: programs for protein crystallography. Acta Crystallogr Sect D Biol Crystallogr 1994;50:760–3.
[39] Emsley P, Lohkamp B, Scott WG, Cowtan K. Features and development of Coot. Acta Crystallogr Sect D Biol Crystallogr 2010;66:486–501.
[40] Xiong Y, Li F, Wang J, Weiner AM, Steitz TA. Crystal structures of an archaeal class I CCA-adding enzyme and its nucleotide complexes. Mol Cell 2003;12:1165–72.
[41] Xiong Y, Steitz TA. Mechanism of transfer RNA maturation by CCA-adding enzyme without using an oligonucleotide template. Nature 2004;430:640–5.
[42] Pan B, Xiong Y, Steitz TA. How the CCA-adding enzyme selects adenine over cytosine at position 76 of tRNA. Science 2010;330:937–40.
[43] Schomaker V, Trueblood KN. On the rigid-body motion of molecules in crystals. Acta Crystallogr Sect B Struct Crystallogr Cryst Chem 1968;24:63–76.
[44] Winn MD, Isupov MN, Murshudov GN. Use of TLS parameters to model anisotropic displacements in macromolecular refinement. Acta Crystallogr Sect D Biol Crystallogr 2001;57:122–33.
[45] Agarwal RC. A new least-squares refinement technique based on the fast Fourier transform algorithm. Acta Crystallogr Sect A Cryst Phys Diffr Theor Gen Crystallogr 1978;34:791–809.
[46] Ten Eyck LF. Crystallographic fast Fourier transforms. Acta Crystallogr Sect A Cryst Phys Diffr Theor Gen Crystallogr 1973;29:183–91.
[47] Kleywegt GJ, Jones TA. xdlMAPMAN and xdlDATAMAN: programs for reformatting, analysis and manipulation of biomacromolecular electron-density maps and reflection data sets. Acta Crystallogr Sect D Biol Crystallogr 1996;52:826–8.
[48] Winn MD, Ballard CC, Cowtan KD, Dodson EJ, Emsley P, Evans PR, et al. Overview of the CCP4 suite and current developments. Acta Crystallogr Sect D Biol Crystallogr 2011;67:235–42.
[49] Cowtan K. Fitting molecular fragments into electron density. Acta Crystallogr Sect D Biol Crystallogr 2008;64:83–9.
[50] French S, Wilson K. On the treatment of negative intensity observations. Acta Crystallogr Sect A Cryst Phys Diffr Theor Gen Crystallogr 1978;34:517–25.